Inorg. Chem. **2008**, *47*, 7556−7567

Chiral Distortion in a $Mn^{IV}(salen)(N_3)_2$ Derived from Jacobsen's Catalyst as a Possible Conformation Model for Its Enantioselective Reactions

Takuya Kurahashi and Hiroshi Fujii*

Institute for Molecular Science & Okazaki Institute for Integrative Bioscience, National Institutes of Natural Sciences, Myodaiji, Okazaki, Aichi 444-8787, Japan

Received March 11, 2008

The $Mn^{IV}(salen)(N_3)_2$ complex (**3**) from Jacobsen's catalyst is synthesized, and the X-ray crystal structures of **3** as well as the starting $Mn^{III}(salen)(N_3)(CH_3OH)$ complex (**2**) are determined in order to investigate the conformation of the high-valent $Mn^{IV}(salen)$ molecule in comparison with that of $Mn^{III}(salen)$. The asymmetric unit of the crystal of **3** contains four complexes, all of which adopt a nonplanar stepped conformation effectively distorted by the chirality of the diimine bridge. The asymmetric unit of **2** also contains four complexes. Two of them show a stepped conformation of a lesser degree, but the other two adopt a bowl-shaped conformation. Comparison of the structural parameters shows that the Mn center in **3** is coordinated from both sides by two external axial N_3 ligands with significantly shorter bond lengths, which could induce greater preference for the stepped conformation in **3**. The CH_3CN solution of **3** shows circular dichroism with a significantly strong band at 275 nm as compared to **2**, suggesting that **3** may adopt a more chirally distorted conformation also in solution. The circular dichroism spectrum of **3** is slightly altered with isodichroic points from 298 to 253 K and shows no further change at temperatures lower than 253 K, suggesting that the solution of **3** contains an equilibrium between two conformers, where a low-energy conformer with more chiral distortion is predominantly favored even at room temperature. Complexes **2** and **3** are thoroughly characterized using various techniques including cyclic voltammetry, magnetic susceptibility, UV−vis, electron paramagnetic resonance, ^1H NMR, infrared spectroscopy, and electrospray ionization mass spectrometry.

Introduction

Since the discovery of a manganese salen complex, Mn(salen), as an epoxidation catalyst by Kochi,[1] a variety of chiral Mn(salen)s have been actively investigated, leading to successful enantioselective transformations of unfunctionalized olefins to chiral epoxides, now known as Jacobsen−Katsuki epoxidation.[2−4] Among chiral Mn(salen)s, a commercially available (*R*,*R*)- and (*S*,*S*)-*N*,*N*′-bis(3,5-di-*tert*-butylsalicylidene)-1,2-cyclohexanediaminomanganese(III) chloride, **1** (Jacobsen's catalyst), is blessed with high levels of enantioselectivity in spite of a relatively simple structure (Scheme 1).[2b] According to the proposal by Kochi, reactions of $Mn^{III}(salen)$ with oxidants such as NaOCl, PhIO, and *m*-chloroperoxybenzoic acid (*m*-CPBA) generate high-valent oxomanganese species $Mn^{V}(salen)(O)$, which transfers the Mn-bound oxygen atom to olefins.[1] In **1**, the diimine bridge is the only chiral unit, which must be responsible for stereochemical communication between $Mn^{V}(salen)(O)$ and incoming substrates in the transition state.

The origin of the stereochemical control by **1** has attracted considerable attention over the past decade. X-ray structural studies of **1** and related chiral $Mn^{III}(salen)$s have shown that the catalyst adopts relatively flat conformations, which are flexibly altered by crystal packing.[5] On the other hand, an X-ray crystal structure of a stable $Mn^{V}(salen)(N)$ from **1**, which could be considered as an appropriate model for the putative $Mn^{V}(salen)(O)$, indeed shows a nonplanar ligand

* Author to whom correspondence should be addressed. E-mail: hiro@ims.ac.jp.

(1) Srinivasan, K.; Michaud, P.; Kochi, J. K. *J. Am. Chem. Soc.* **1986**, *108*, 2309–2320.

(2) (a) Zhang, W.; Loebach, J. L.; Wilson, S. R.; Jacobsen, E. N. *J. Am. Chem. Soc.* **1990**, *112*, 2801–2803. (b) Jacobsen, E. N.; Zhang, W.; Muci, A. R.; Ecker, J. R.; Deng, L. *J. Am. Chem. Soc.* **1991**, *113*, 7063–7064.

(3) Irie, R.; Noda, K.; Ito, Y.; Katsuki, T. *Tetrahedron Lett.* **1991**, *32*, 1055–1058.

(4) For a review, see: (a) McGarrigle, E. M.; Gilheany, D. G. *Chem. Rev.* **2005**, *105*, 1563–1602.

(5) Pospisil, P. J.; Carsten, D. H.; Jacobsen, E. N. *Chem.—Eur. J.* **1996**, *2*, 974–980.

10.1021/ic800443q CCC: $40.75
Published on Web 08/02/2008

Scheme 1. Syntheses of **2** and **3**

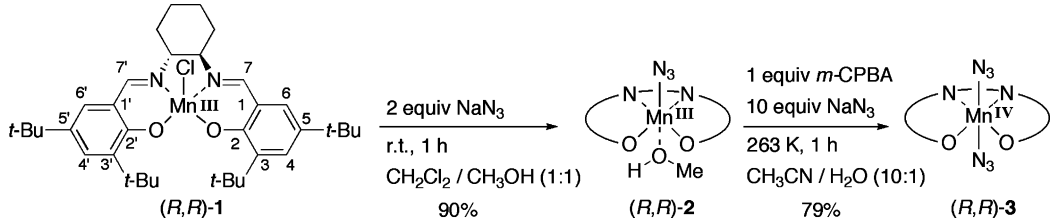

structure, in which one *tert*-butyl group at the 3 position points down and the other at the 3′ position points up for one of two complexes in the asymmetric unit.[6] But this may not account for the stereochemical control, because the other complex shows an exactly opposite distortion, suggesting again flexibility of the salen ligand irrespective of the Mn valency. Highly enantioselective reactions carried out by the seemingly flat and flexible Jacobsen's catalyst are quite puzzling, while Katsuki's second-generation Mn(salen)s bearing additional axial chirality at the 3 and 3′ positions were well studied from the viewpoint of catalyst conformation.[7,8] The conformations of other optically active Mn(salen)s were also investigated to elucidate the mechanism of asymmetric catalytic reactions.[9]

In most of the previous models, to explain high stereochemical control by Jacobsen's catalyst, the chirality of the diimine bridge is assumed to be transmitted to the two salicylidene rings only upon formation of the putative $Mn^{V}(salen)(O)$, leading to significant chiral distortion for effective stereochemical communications.[4] Inspection of X-ray crystal structures of $Cr^{V}(salen)(O)$[10] and Al(salen)[11] in achiral salen frameworks leads to the proposal of three principal nonplanar conformations: stepped, bowl-shaped, and bent conformations.[12] Stepped and bowl-shaped conformations bear distorted salicylidene rings relative to the basal N_2O_2 ligand plane. The bent conformation is distinct from the other two, with one of the phenolate oxygens in an apical position. In addition, a twist of the salicylidene rings is also considered in each of these three conformations. Theoretical investigations supported distortion from planarity of the salen ligand upon the formation of $Mn^{V}(salen)(O)$,[13] and one of these investigations further pointed out that the coordination of an axial ligand might be critical in inducing effective chiral distortion in $Mn^{V}(salen)(O)$.[13d] However, the absence of structural insight for Jacobsen's catalyst in a chirally distorted conformation hampers more detailed discussion. It is also quite interesting to know how the flat and flexible Jacobsen's catalyst can adopt a rigid chiral conformation for highly enantioselective reactions only upon formation of an active intermediate.

As a part of our efforts to study high-valent intermediates from salen complexes,[14] we herein describe the conformation of the high-valent Jacobsen's Mn(salen). In order to stabilize a high-valent Mn center, axial N_3 ligands are incorporated, following the previous example of the high-valent Fe complex.[15] We successfully obtained an X-ray crystal structure of the six-coordinate $Mn^{IV}(salen)(N_3)_2$, **3**. While several Mn^{IV} complexes from Schiff base ligands have been structurally characterized,[16] they are commonly not mononuclear, and thus a mononuclear Mn^{IV} complex **3** is worth investigating. Quite interestingly, all of **3** in the asymmetric unit adopts a stepped conformation, while the six-coordinate $Mn^{III}(salen)(N_3)(CH_3OH)$, **2**, which is one-electron reduced from **3**, exhibits a mixture of stepped and bowl-shaped conformations. The solution structure is investigated with circular dichroism (CD) spectroscopy, in comparison with a very recent solid-state and solution study on the chiral Ni(salen)s reported by Fox and co-workers, where the solution structures were rigorously established.[17] The CH_3CN solution of **3** shows CD with a significantly strong band at 275 nm as compared to **2**, suggesting that **3** may adopt a more chirally distorted conformation also in solution. The CD of **3** shows little temperature-dependence with isodichroic

(6) (a) Svenstrup, N.; Bøgevig, A.; Hazell, R. G.; Jørgensen, K. A. *J. Chem. Soc., Perkin Trans. 1* **1999**, 1559–1565. (b) Ho, C.-M.; Lau, T.-C.; Kwong, H.-L.; Wong, W.-T. *J. Chem. Soc., Dalton Trans.* **1999**, 2411–2413.

(7) For a review, see: Katsuki, T. *Adv. Synth. Catal.* **2002**, *344*, 131–147.

(8) (a) Nishikori, H.; Ohta, C.; Oberlin, E.; Irie, R.; Katsuki, T. *Tetrahedron* **1999**, *55*, 13937–13946. (b) Hashihayata, T.; Punniyamurthy, T.; Irie, R.; Katsuki, T.; Akita, M.; Moro-oka, Y. *Tetrahedron* **1999**, *55*, 14599–14610.

(9) Hirotsu, M.; Nakajima, K.; Kojima, M.; Yoshikawa, Y. *Inorg. Chem.* **1995**, *34*, 6173–6178.

(10) Samsel, E. G.; Srinivasan, K.; Kochi, J. K. *J. Am. Chem. Soc.* **1985**, *107*, 7606–7617.

(11) Atwood, D. A.; Jegier, J. A.; Rutherford, D. *J. Am. Chem. Soc.* **1995**, *117*, 6779–6780.

(12) For proposed conformations of Mn(salen)'s, see ref 4.

(13) (a) Houk, K. N.; DeMello, N. C.; Condroski, K.; Fennen, J.; Kasuga, T. *Proceedings of the ECHET96 Electronic Conference*, 1996. http://www.ch.ic.ac.uk/ectoc/echet96 (accessed July 2008). (b) Strassner, T.; Houk, K. N. *Org. Lett.* **1999**, *1*, 419–421. (c) Jacobsen, H.; Cavallo, L. *Chem.—Eur. J.* **2001**, *7*, 800–807. (d) El-Bahraoui, J.; Wiest, O.; Feichtinger, D.; Plattner, D. A. *Angew. Chem., Int. Ed.* **2001**, *40*, 2073–2076. (e) Lipkowitz, K. B.; Schefzick, S. *Chirality* **2002**, *14*, 677–682. (f) Cavallo, L.; Jacobsen, H. *J. Org. Chem.* **2003**, *68*, 6202–6207. (g) Khavrutskii, I. V.; Musaev, D. G.; Morokuma, K. *Proc. Natl. Acad. Sci. U.S.A.* **2004**, *101*, 5743–5748.

(14) (a) Kurahashi, T.; Kobayashi, Y.; Nagatomo, S.; Tosha, T.; Kitagawa, T.; Fujii, H. *Inorg. Chem.* **2005**, *44*, 8156–8166. (b) Kurahashi, T.; Kikuchi, A.; Tosha, T.; Shiro, Y.; Kitagawa, T.; Fujii, H. *Inorg. Chem.* **2008**, *47*, 1674–1686.

(15) Berry, J. F.; Bill, E.; Bothe, E.; Weyhermüller, T.; Wieghardt, K. *J. Am. Chem. Soc.* **2005**, *127*, 11550–11551.

(16) For a mononuclear complex, see: Law, N. A.; Machonkin, T. E.; McGorman, J. P.; Larson, E. J.; Kampf, J. W.; Pecoraro, V. L. *J. Chem. Soc., Chem. Commun.* **1995**, 2015–2016. For dinuclear complexes, see: (a) Gohdes, J. W.; Armstrong, W. H. *Inorg. Chem.* **1992**, *31*, 368–373. (b) Larson, E.; Lah, M. S.; Li, X.; Bonadies, J. A.; Pecoraro, V. L. *Inorg. Chem.* **1992**, *31*, 373–378. (c) Torayama, H.; Nishide, T.; Asada, H.; Fujiwara, M.; Matsushita, T. *Polyhedron* **1998**, *17*, 105–118. (d) Law, N. A.; Kampf, J. W.; Pecoraro, V. L. *Inorg. Chim. Acta* **2000**, *297*, 252–264. (e) Maneiro, M.; Bermejo, M. R.; Fondo, M.; González, A. M.; Sanmartín, J.; García-Monteagudo, J. C.; Pritchard, R. G.; Tyryshkin, A. M. *Polyhedron* **2001**, *20*, 711–719.

(17) Dong, Z.; Yap, G. P. A.; Fox, J. M. *J. Am. Chem. Soc.* **2007**, *129*, 11850–11853.

Table 1. Crystallographic Data for **2** and **3**

	2	**3**
formula	$C_{151}H_{229}Mn_4N_{20}O_{15}$	$C_{148}H_{216}Cl_8Mn_4N_{32}O_8$
M_r	2784.35	3074.92
T/K	173	173
cryst size/mm	0.40 × 0.30 × 0.20	0.30 × 0.20 × 0.05
cryst syst	monoclinic	monoclinic
space group	$C2$ (No. 5)	$P2_1$ (No. 4)
cryst color	red	dark red
λ/Å	0.71070	0.71070
μ/mm^{-1}	0.373	0.498
a/Å	26.7314(3)	14.707(4)
b/Å	18.2202(5)	24.208(7)
c/Å	32.6736(5)	22.818(6)
α/deg	90.0000	90.0000
β/deg	91.8940(14)	90.1332(13)
γ/deg	90.0000	90.0000
V/Å^3	15905.0(5)	8124(4)
Z value	4	2
D_{calc}/g cm^{-3}	1.163	1.257
GOF	1.020	1.054
R_1[a]	0.0667	0.0828
R_w[b]	0.1796	0.2644
Flack	0.043(16)	0.13(2)

[a] $R_1 = \sum||F_o| - |F_c||/\sum|F_o|$. [b] $R_w = [\sum w(F_o^2 - F_c^2)^2/\sum w(F_o^2)^2]^{1/2}$.

points in the range from 298 to 253 K, suggesting that the solution of **3** contains an equilibrium between two conformers, where a low-energy conformer with more chiral distortion is predominantly favored even at room temperature. The conformation of **3** could serve as a potentially useful model to precisely predict stereochemical communications between Jacobsen's Mn(salen) and various substrates. We also carried out a thorough spectroscopic characterization of **2** and **3**, using cyclic voltammetry, magnetic susceptibility, UV−vis, electron paramagnetic resonance (EPR), ^{1}H NMR, infrared (IR) spectroscopy, and electrospray ionization mass (ESI-MS) spectrometry. A comparison of structural parameters and spectroscopic properties between **2** and **3** reveals key factors for the chiral distortion of Jacobsen's catalyst.

Results

Syntheses of 2 and 3. As summarized in Scheme 1, **2** was synthesized by the reaction of **1** with 2 equiv of NaN_3 in $CH_2Cl_2-CH_3OH$ (1:1) for 1 h at room temperature. Recrystallization from hot CH_3CN gave analytically pure **2** in 90% yield. Complex **3** was synthesized from **2** by reaction with 1 equiv of *m*-CPBA and 10 equiv of NaN_3 in CH_3CN-H_2O (10:1) for 1 h at 263 K. Analytically pure **3** was obtained in 79% yield after recrystallization from CH_2Cl_2−pentane at 253 K.

X-Ray Crystal Structures of 2 and 3. The crystal structures of **2** and **3** were determined by X-ray crystallography, and the crystallographic data are summarized in Table 1. The asymmetric units of both **2** and **3** contain four mononuclear complexes, **2a**−**d** and **3a**−**d**, and the packing diagrams for **2** and **3** are shown in Figure 1. Tables 2 and 3 summarize selected structural parameters of **2a**−**d** and **3a**−**d**, respectively. Tables 2 and 3 also include parameters α and β, which are defined as angles between the planes of the salicylidene rings and the least-squares plane of the N_2O_2 of the salen ligand for quantitative comparison as shown in Figure 2.[4] In order to compare the mutual orientation of the two salicylidene rings in the salen complex, we define the

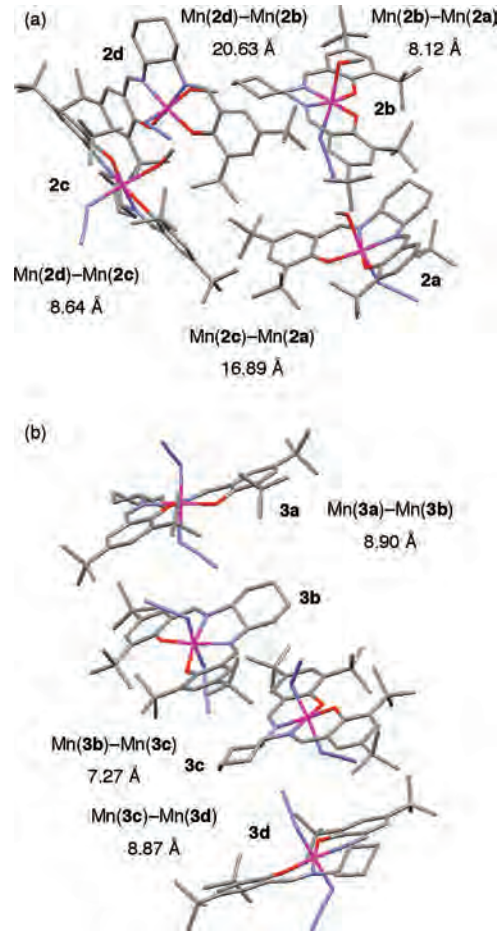

Figure 1. Packing diagrams for (a) (*R*,*R*)-**2** and (b) (*R*,*R*)-**3**. Hydrogen atoms and noncoordinated solvent molecules are omitted for the sake of clarity.

Table 2. Selected Structural Parameters for **2a**−**d**

	2a	**2b**	**2c**	**2d**
α/deg	185.7	164.5	165.9	188.2
β/deg	159.5	171.4	169.0	161.0
γ/deg	−4.7	16.3	−5.2	9.4
Mn−N_2O_2 plane/Å	0.09	0.08	0.07	0.09
Mn−O1/Å	1.875(3)	1.872(3)	1.874(3)	1.882(3)
Mn−O2/Å	1.871(3)	1.877(3)	1.894(3)	1.868(3)
Mn−N1/Å	1.976(4)	1.990(4)	1.987(4)	1.996(4)
Mn−N2/Å	1.975(4)	1.978(4)	1.994(4)	1.987(4)
Mn−N3/Å	2.256(5)	2.177(5)	2.203(4)	2.221(5)
Mn−O3/Å	2.349(4)	2.373(4)	2.338(4)	2.372(4)
N3−N4/Å	1.155(8)	1.155(7)	1.177(7)	1.172(8)
N4−N5/Å	1.155(10)	1.167(7)	1.172(7)	1.182(10)
O1−C2/Å	1.322(5)	1.333(6)	1.307(6)	1.313(6)
O2−C2′/Å	1.320(6)	1.309(6)	1.309(7)	1.305(6)
N1−C7/Å	1.288(6)	1.283(6)	1.287(7)	1.274(7)
N2−C7′/Å	1.291(6)	1.286(6)	1.281(7)	1.274(6)
C1−C7/Å	1.427(7)	1.431(7)	1.441(8)	1.459(9)
C1′−C7′/Å	1.414(8)	1.449(7)	1.440(8)	1.457(7)
O1−Mn−N2/deg	174.06(17)	173.32(17)	172.23(17)	173.36(18)
O2−Mn−N1/deg	170.48(17)	171.17(16)	173.48(17)	170.49(17)
N3−N4−N5/deg	178.4(7)	176.5(5)	174.6(5)	179.8(7)
Mn−N3−N4/deg	119.0(4)	142.5(4)	125.7(3)	115.1(4)

torsion angle γ, which shows the twist of the salicylidene rings.

As seen from the packing diagram in Figure 1a, the shortest intermolecular Mn−Mn distance among **2a**−**d** is 8.12 Å. All of **2a**−**d** are six-coordinate complexes bearing an azide and a solvent methanol as axial ligands, but the conformations of **2a**−**d** significantly differ from each other,

Table 3. Selected Structural Parameters for **3a**−**d**

	3a	3b	3c	3d
α/deg	155.5	150.0	162.6	159.9
β/deg	150.0	154.1	160.3	164.0
γ/deg	4.1	4.1	−6.7	−8.6
Mn−N_2O_2 plane/Å	0.00	0.02	0.00	0.01
Mn−O1/Å	1.853(5)	1.863(4)	1.878(4)	1.844(5)
Mn−O2/Å	1.873(5)	1.840(5)	1.842(4)	1.864(4)
Mn−N1/Å	1.983(5)	1.984(6)	1.968(5)	1.969(5)
Mn−N2/Å	1.982(6)	1.986(6)	1.963(5)	1.983(6)
Mn−N3/Å	2.006(6)	1.980(6)	1.958(7)	1.989(6)
Mn−N6/Å	1.974(6)	1.964(6)	1.974(7)	1.975(6)
N3−N4/Å	1.212(8)	1.210(9)	1.201(9)	1.209(9)
N4−N5/Å	1.144(9)	1.137(10)	1.131(11)	1.131(11)
N6−N7/Å	1.219(9)	1.242(9)	1.228(9)	1.202(8)
N7−N8/Å	1.136(10)	1.142(10)	1.139(10)	1.154(10)
O1−C2/Å	1.348(8)	1.360(8)	1.349(8)	1.358(9)
O2−C2′/Å	1.330(8)	1.349(8)	1.331(9)	1.331(8)
N1−C7/Å	1.269(9)	1.291(9)	1.298(9)	1.294(9)
N2−C7′/Å	1.282(9)	1.300(9)	1.297(8)	1.290(9)
C1−C7/Å	1.469(9)	1.436(10)	1.438(9)	1.438(9)
C1′−C7′/Å	1.448(10)	1.420(9)	1.421(9)	1.446(10)
O1−Mn−N2/deg	172.2(2)	171.9(2)	173.5(2)	173.6(2)
O2−Mn−N1/deg	172.4(2)	173.5(2)	173.0(2)	173.3(2)
N3−N4−N5/deg	175.0(7)	174.5(7)	177.4(9)	175.1(8)
N6−N7−N8/deg	173.5(7)	176.9(7)	175.9(8)	176.4(9)
Mn−N3−N4/deg	117.6(5)	118.3(4)	119.6(5)	120.0(5)
Mn−N6−N7/deg	117.2(4)	119.2(5)	121.3(5)	117.4(5)

indicating once again the conformational flexibility of Jacobsen's catalyst. The conformations of **2a** and **2d** are categorized as bowl-shaped, which is in clear contrast to a stepped conformation for **2b** and **2c**.[12] Figure 2 shows X-ray crystal structures of **2a** and **2b** in bowl-shaped and stepped conformations, respectively. Then, the structural parameters of **2a/2d** and **2b/2c**, summarized in Table 2, are carefully compared, and we pinpoint the Mn−N3(N_3) bond length as the only significant difference between the stepped and bowl-shaped conformations; the Mn−N3(N_3) bond length in the bowl-shaped **2a/2d** is slightly longer (2.256 and 2.221 Å) than that in the stepped **2b/2c** (2.177 and 2.203 Å). It is also interesting to note that the N3−N4−N5 angles in the Mn-coordinated N_3 ions are different between **2a/2d** (178.4 and 179.8 °) and **2b/2c** (176.5 and 174.6 °). The shorter Mn−N3(N_3) bond length may affect the N3−N4−N5 angle in **2b** and **2c**, as well as the Mn−N3−N4 angle in **2b**, which considerably deviates from 120°. The torsion angles γ of **2a**−**d** show a slight twist of the salicylidene rings, but the direction of the twist is different between **2a/2c** and **2b/2d**, indicating that the twist of the salicylidene rings is not induced by the chirality of the diimine bridge, but is rather a consequence of the crystal packing.

The packing diagram for **3** in Figure 1b shows that the shortest intermolecular Mn−Mn distance is 7.27 Å, suggesting similar intermolecular contacts when compared to **2**. In contrast to **2**, all of **3a**−**d** exhibit a stepped conformation, indicative of a considerable preference for this conformation. In addition, the degree of a stepped conformation in **3a**−**d** is more remarkable than **2b/2c**, as judged from angles α and β summarized in Tables 2 and 3. Figure 2 shows the structure of **3a**. As shown from the structural parameters of **3a**−**d** in Table 3, the Mn−N_{azide} bond length becomes much shorter (1.958−2.006 Å for **3a**−**d** versus 2.177/2.203 Å for **2b/2c**). This structural feature could be correlated with a greater preference of **3a**−**d** for a stepped conformation, in agreement with the observation for the

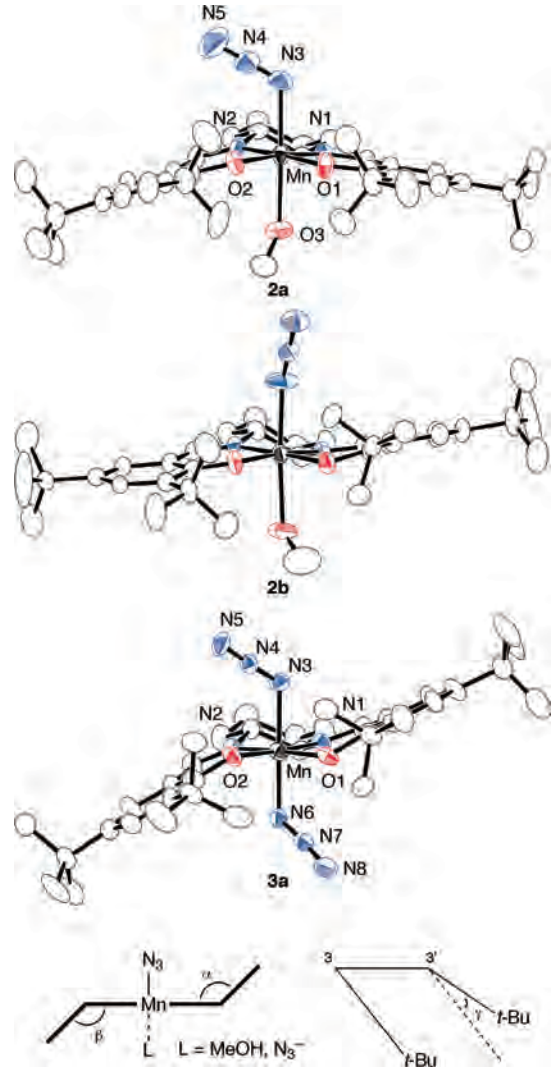

Figure 2. X-ray crystal structures of (*R*,*R*)-**2a,** (*R*,*R*)-**2b**, and (*R*,*R*)-**3a**. Thermal ellipsoids represent the 50% probability surfaces. Hydrogen atoms are omitted for the sake of clarity. The angles α and β are defined as those between the planes of the salicylidene rings and the least-squares plane of the N_2O_2 of the salen ligand. The angle γ is a twist angle between two *tert*-butyl groups at the 3 and 3′ positions.

difference between the bowl-shaped **2a/2d** and the stepped **2b/2c**. Among **3a**−**d**, **3a** and **3b** exhibit a greater degree of a stepped conformation than **3c** and **3d**. This might be possibly due to a difference in packing in the crystal, because there is no detectable difference in the structural parameters between **3a/3b** and **3c/3d**. A remarkable change on going from Mn^{III} to Mn^{IV} is unsymmetrical N_3 ligands in **3a**−**d**, and the N_α−N_β (N3−N4 and N6−N7) bond lengths are 1.201−1.242 Å, which are longer than the N_β−N_γ (N4−N5 and N7−N8) bond lengths (1.131−1.154 Å). This is in clear contrast to **2b/2c**, which have symmetrical N_3 ions (the N3−N4 bond length, 1.155−1.177 Å; the N4−N5 bond length, 1.167−1.172 Å). In spite of a significant bond length change, the N_α−N_β−N_γ angles in **3a**−**d** (173.5−177.4 °) are almost the same as those in **2b/2c** (176.5/174.6 °). The Mn−O1(O2)/Mn−N1(N2) bond lengths are different between **3a**−**d** (1.840−1.878/1.963−1.986 Å) and **2b/2c** (1.872−1.894/1.978−1.994 Å). Shorter Mn−O1(O2)/Mn−N1(N2) bonds in **3a**−**d** are probably correlated with a smaller

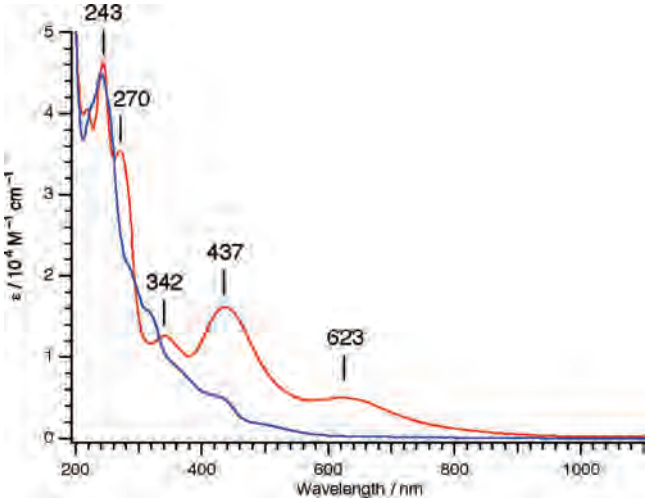

Figure 3. UV−vis spectra of (*R*,*R*)-**2** (blue line) and (*R*,*R*)-**3** (red line) in CH_3CN (0.04 mM) at room temperature.

displacement of the Mn center from the basal ligand plane. Another slight but significant difference on going from Mn^{III} to Mn^{IV} is the phenolate C−O bond length, which is in the range of 1.307−1.333 Å for **2b/2c** and 1.330−1.360 Å for **3a**−**d**. The other structural parameters for the salen ligand, including the imine C=N and C1−C7 bond lengths, do not change, suggesting that the π system of the salen ligand is not altered significantly. Comparison of the torsion angle γ shows that the salicylidene rings are slightly twisted in different directions between **3a/3b** and **3c/3d**.

Solution Studies of 2 and 3. UV−vis spectra of **2** and **3** were measured in CH_3CN at room temperature (Figure 3). The UV−vis spectra of **3** in CH_3CN, CH_3OH, and CH_2Cl_2 do not change for several hours at room temperature, although standing the solution of **3** for several days at room temperature results in gradual decomposition. Upon the oxidation of **2** to **3**, absorptions appear at 270, 342, 437, and 623 nm (ε = 35 000, 12 600, 16 200, and 5000 $M^{-1}cm^{-1}$). A Mn^{IV}(2,2′-bipyridine)$(N_3)_4$ complex was reported to exhibit UV−vis absorptions at 290 and 442 nm (ε = 33 000 and 22 000 $M^{-1}cm^{-1}$), which were assigned as the charge transfer bands from N_3 to Mn^{IV}.[18] It was also reported that a mononuclear Mn^{IV} Schiff base complex exhibits UV−vis absorptions at 310 and 580 nm (ε = 16 100 and 3350 $M^{-1}cm^{-1}$), which are apparently absent for the starting Mn^{III} complex.[19] Our previous study on a sterically hindered Mn(salen) showed that Mn^{IV}(salen) complexes bearing =O, −OH, $-OCH_3$, and −Cl as an external axial ligand exhibit a characteristic absorption at 600−730 nm (ε = 5000−6000 $M^{-1}cm^{-1}$).[14b] According to these studies, the absorption feature at 623 nm for **3**, which is common for the Mn^{IV}−phenolate moiety, could be assigned to the phenolate-to-Mn^{IV} charge transfer band. The absorption at 437 nm for **3** is similar to the absorption at 442 nm reported for the Mn^{IV}(2,2′-bipyridine)$(N_3)_4$ complex and thus might be assigned as the N_3-to-Mn^{IV} charge transfer band. The

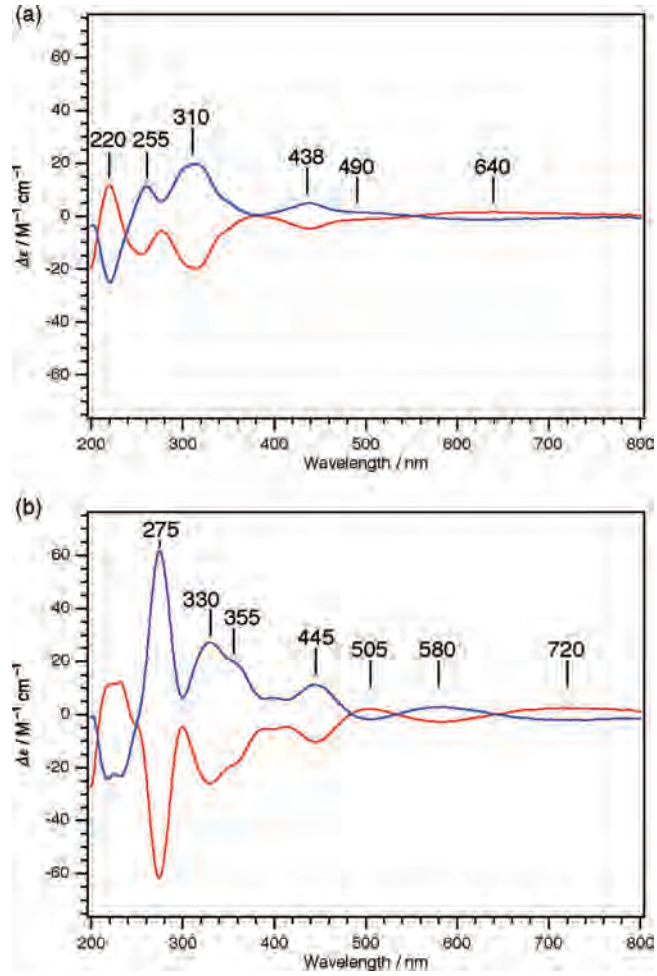

Figure 4. Circular dichroism spectra of (a) (*R*,*R*)-**2** (red line) and (*S*,*S*)-**2** (blue line) and (b) (*R*,*R*)-**3** (red line) and (*S*,*S*)-**3** (blue line) in CH_3CN (0.04 mM) at room temperature.

absorptions at 342, 270, and 243 nm for **3** could mainly arise from the salen ligand, in comparison with a UV−vis spectrum of the metal-free ligand with absorption maxima at 329, 260, and 219 nm (ε = 7300, 19 000, and 43 000 $M^{-1}cm^{-1}$), as shown in Figure S1 (Supporting Information). Among these absorptions, the absorption at 342 nm is assigned as the $\pi-\pi^*$ transition of the azomethine group, while the absorptions at 270 and 243 nm are assigned as the $\pi-\pi^*$ transition of the phenolates (*vide infra*).

Figure 4 shows CD spectra of **2** and **3** in CH_3CN at room temperature. The most notable feature is intense negative and positive CD bands at 275 nm ($|\Delta\varepsilon|$ = 61.6 $M^{-1}cm^{-1}$) for (*R*,*R*)-**3** and (*S*,*S*)-**3**. CD bands at 255 nm for **2** ($|\Delta\varepsilon|$ = 14.4 $M^{-1}cm^{-1}$), which may come from the same origin, are considerably weak. The difference of CD between **2** and **3** should arise from chiroptical properties as mononuclear species, not as polynuclear species through a possible bridging ligand N_3, because CD spectra of **2** and **3** in 0.04 and 0.4 mM concentrations as shown in Figures 4 and 5, respectively, do not differ significantly when a coordinating CH_3CN solvent is utilized. On the other hand, when a noncoordinating CH_2Cl_2 solvent is utilized, a sign of the CD band at 220 nm for (*R*,*R*)-**2** is inverted, suggesting that some intermolecular interaction may contribute to a chiroptical

(18) Dave, B. C.; Czernuszewicz, R. S. *J. Coord. Chem.* **1994**, *33*, 257–269.
(19) Chandra, S. K.; Basu, P.; Ray, D.; Pal, S.; Chakravorty, A. *Inorg. Chem.* **1990**, *29*, 2423–2428.

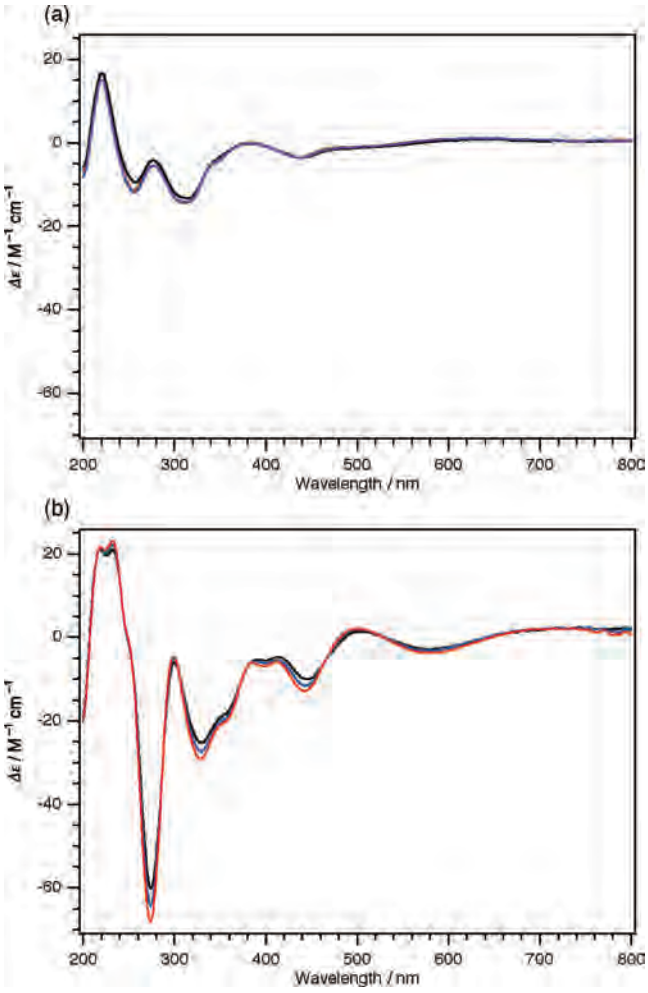

Figure 5. Circular dichroism spectra of (a) (*R*,*R*)-**2** and (b) (*R*,*R*)-**3** in CH_3CN (0.4 mM) at 298 (black line), 273 (blue line), and 253 K (red line).

property even in a 0.04 mM concentration (Figure S2, Supporting Information). However, CD spectra of **3** in CH_2Cl_2 are almost identical with those in CH_3CN, indicating again that the intense CD bands at 275 nm arise form chiroptical properties as a mononuclear complex. This is possibly because **3**, which is a bis-azide complex, does not have a coordination site available for bridging, while a CH_3OH ligand in **2** could be replaced by a N_3 ligand in another molecule.

Figures 5 and 6 show variable-temperature CD and ^{1}H NMR spectra of (*R*,*R*)-**2** and (*R*,*R*)-**3**. As the temperature of the sample is decreased from 298 to 253 K, a CD spectrum of (*R*,*R*)-**3** in CH_3CN is slightly altered with isodichroic points (Figure 5b), indicative of two conformers equilibrating at room temperature. Further cooling of the sample to 243 K induces no change, suggesting one of two conformers is predominant at 253 K. Temperature dependence at higher temperatures above 313 K could not be measured due to the gradual decomposition of **3**. On the other hand, CD of **2** shows an almost negligible temperature dependence (Figure 5a).

Some of ^{1}H NMR signals of **2** and **3**, which bear paramagnetic high-spin d^4 Mn^{III} and d^3 Mn^{IV} centers, appear at largely shifted positions. Complex **2** shows ^{1}H NMR signals at 17.3, 8.3, −24.0, and −27.5 ppm (Figure 7a). The

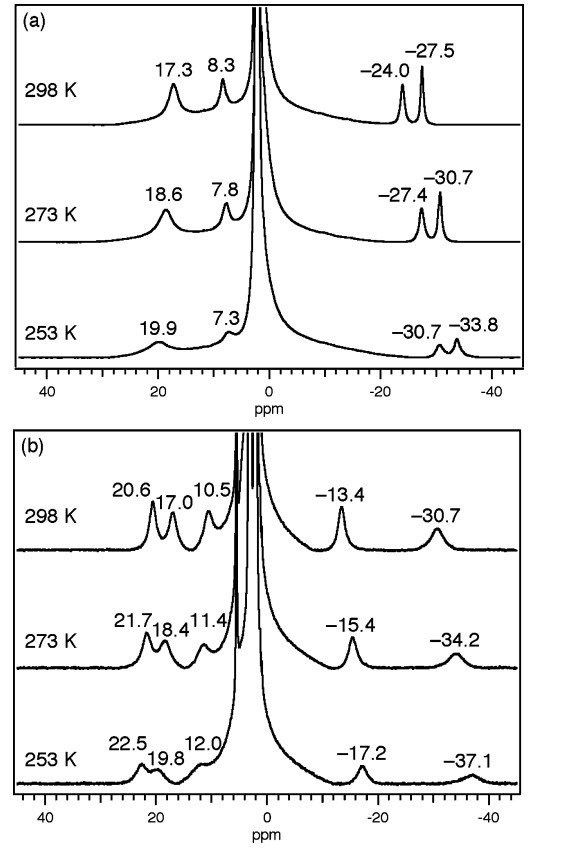

Figure 6. ^{1}H NMR spectra of (a) (*R*,*R*)-**2** and (b) (*R*,*R*)-**3** in CD_3CN (10 mM) at 298, 273, and 253 K.

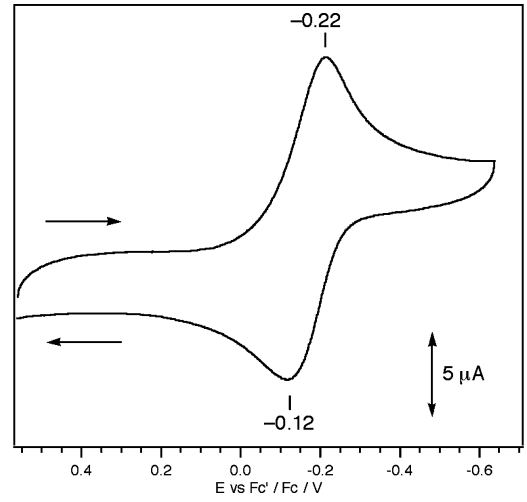

Figure 7. Cyclic voltammogram of **3** in CH_3CN under an Ar atmosphere at room temperature. Conditions: 1×10^{-3} M of **3**; 0.10 M Bu_4NClO_4 supporting electrolyte; a saturated calomel reference electrode; a glassy carbon working electrode; a platinum-wire counter electrode; scan rate 50 mV s^{-1}. The potentials are referenced versus the ferrocenium/ferrocene (Fc′/Fc) couple.

signals at −24.0 and −27.5 ppm, which shift upfield upon decreasing the temperature, could be assigned to the 4H and 4′H of the aromatic rings according to the previous studies (for numbering of the aromatic rings, see Scheme 1).[20,21a] The signal at 17.3 ppm, which apparently bears doubled integrated intensity as compared to the signals at −24.0 and

(20) Bonadies, J. A.; Maroney, M. J.; Pecoraro, V. L. *Inorg. Chem.* **1989**, *28*, 2044–2051.

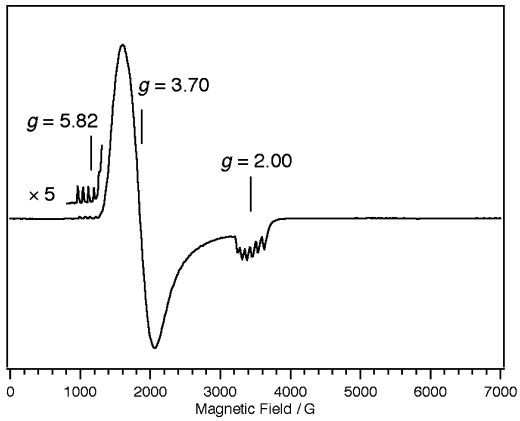

Figure 8. X band EPR spectrum of **3** in frozen CH_2Cl_2−toluene (7:3) at 4 K. Conditions: microwave frequency, 9.56 GHz; microwave power, 2.012 mW; modulation amplitude, 7 G; time constant, 163.84 ms; conversion time, 163.84 ms.

−27.5 ppm and moves downfield at lower temperatures, could be assigned to the 6H and 6′H of the aromatic rings. The signal at 8.3 ppm, which shifts upfield upon decreasing the temperature, could not be assigned. Assuming a similar effect between Mn^{III} and Mn^{IV}, the signals at −13.4/−30.7 ppm and 17.0/20.6 ppm for **3** could be assigned to 4/4′H and 6/6′H, respectively. Separate signals for 4/4′H and 6/6′H even at 253 K are indicative of unequivalent aromatic rings in solution, which are inconsistent with an ideal stepped conformation.

ESI-MS spectrometry of **3** in the presence of 1 equiv of sodium trifluoromethanesulfonate (NaOTf) and 18-crown-6 in CH_2Cl_2 gives a singly charged signal at *m*/*z* 970.56 (Figure S3, Supporting Information), which arises from an adduct of **3** and Na^+−18-crown-6. This implies that **3** exists as a bis-azide complex also in solution. The IR spectrum of **3** also supports that **3** is a bis-azide form in the CH_3CN solution, just as revealed by X-ray crystallography (*vide infra*).

Spectroscopic Properties of Crystallographically-Characterized Mn^{III}(salen) and Mn^{IV}(salen). Cyclic voltammetry of **3** shows a reversible redox wave at $E_{1/2} = -0.17$ V (calculated as the average of anodic and cathodic peak potentials) versus the ferrocenium/ferrocene couple (Fc′/Fc), as shown in Figure 7. A controlled-potential reduction of **3** at a voltage of −0.54 V versus Fc′/Fc at room temperature generates **2** after UV−vis spectral changes with clear isosbestic points (Figure S4, Supporting Information), indicating that the redox wave at $E_{1/2} = -0.17$ V corresponds to the reduction of Mn^{IV} to Mn^{III} with a concomitant loss of one N_3 ligand. The EPR spectrum of **3** at 4 K shown in Figure 8 exhibits one set of signals at $g = 3.70$ and 2.00 along with a weak signal at $g = 5.82$, which is typical of an $S_t = 3/2$ spin system ($E/D \approx 0$).[14b,21] The signals at $g = 5.82$ and 2.00 display a six-line hyperfine splitting with $A = 78.2$ and 68.5 G, respectively, as expected for the $I = 5/2$ ^{55}Mn nucleus. Temperature dependence of the signals at $g = 3.70/2.00$ and 5.82, which arises from the $m_s = \pm 1/2$ and $\pm 3/2$ doublets of an $S = 3/2$ spin system, respectively, indicates an axial zero-field splitting $D = 0.7$ cm^{-1} (Figure S5, Supporting Information). This value for D is also confirmed by a magnetic susceptibility measurement (*vide infra*). Therefore, **3** belongs to the $S = 3/2$ spin system of large axial distortion ($2D \gg h\nu$, $h\nu = 0.31$ cm^{-1} at the X-band frequency), which is consistent with the form of the EPR signals (strong $g = 3.70$ and weak $g = 2.00$ resonances) in an axial field ($E/D = 0$).[22] Although EPR signals of d^4 Mn^{III}(salen) bearing Cl and H_2O as an external ligand were indeed detected at the conventional X-band frequency,[14b,21c] EPR signals from **2** could not be observed clearly. The absence of EPR signals for **2** is possibly because the D value of **2** is significantly altered upon N_3 binding, as previously reported for N_3-treated MnSOD.[23]

Figure 9b shows a plot of the product of the molar magnetic susceptibility and temperature ($\chi_m T$) versus temperature (T) as well as the reciprocal magnetic susceptibility (χ_m^{-1}) versus T for a polycrystalline sample of **3**. The magnetic susceptibility above 30 K can be well fit to the Curie−Weiss law (eq 1)[24] with the Curie constant $C = 1.82$ cm^3 mol^{-1} K and the Weiss temperature $\theta = -0.55$ K.

$$\frac{1}{\chi_m} = \frac{1}{C}T - \frac{\theta}{C} \tag{1}$$

The C value is close to 1.876 cm^3 mol^{-1} K, which is expected for a high-spin d^3 Mn^{IV} ion in an $S = 3/2$ state. The very small θ value is indicative of a very weak magnetic interaction between Mn^{IV} ions. Thus, the $\chi_m T$ versus T plot could be simulated by the expression for the molar susceptibility of an $S = 3/2$ system that exhibits an axial zero-field splitting D (E = 0):[24]

$$\mathbf{H} = g\beta SH + D\left[S_z^2 - \frac{S(S+1)}{3}\right] + E(S_x^2 - S_y^2)$$

$$\chi_m T = \frac{Ng^2\beta^2}{3k}\frac{1 + 9\exp(-2D/kT)}{4[1 + \exp(-2D/kT)]} + \frac{2Ng^2\beta^2}{3k}\frac{1 + (3kT/4D)[1 - \exp(-2D/kT)]}{1 + \exp(-2D/kT)} \tag{2}$$

where N is the Avogadro number, g is the g factor, β is the Bohr magneton, and k is the Boltzmann constant.

A satisfactory fit, displayed in Figure 9b, was obtained with $D = 0.7$ cm^{-1} and $g = 1.97$. The D values obtained from EPR and SQUID measurements for **3** are thus consistent. On the other hand, the magnetic susceptibility above 50 K for the polycrystalline sample of **2** was fit to the Curie−Weiss law (eq 1) with $C = 3.03$ cm^3 mol^{-1} K and $\theta = -10.1$ K, as shown in Figure 9a. The C value of 3.03 cm^3 mol^{-1} K is close to the spin only value for a high-spin d^4 Mn^{III} ion in an $S = 2$ state (3.001 cm^3 mol^{-1} K). In contrast to **3**, a negative θ value may suggest an antiferromagnetic exchange interaction between neighboring Mn^{III} ions, although the packing diagram of **2** shows relatively long Mn−Mn distances just as in the case of **3** (Figure 1). As recently reported for a similar system prepared from Mn^{III}(salen)$(N_3)(CH_3OH)$,[25] the sixth coordination site on

(21) (a) Bryliakov, K. P.; Babushkin, D. E.; Talsi, E. P. *J. Mol. Catal. A* **2000**, *158*, 19–35. (b) Adam, W.; Mock-Knoblauch, C.; Saha-Möller, C. R.; Herderich, M. *J. Am. Chem. Soc.* **2000**, *122*, 9685–9691. (c) Campbell, K. A.; Lashley, M. R.; Wyatt, J. K.; Nantz, M. H.; Britt, R. D. *J. Am. Chem. Soc.* **2001**, *123*, 5710–5719.

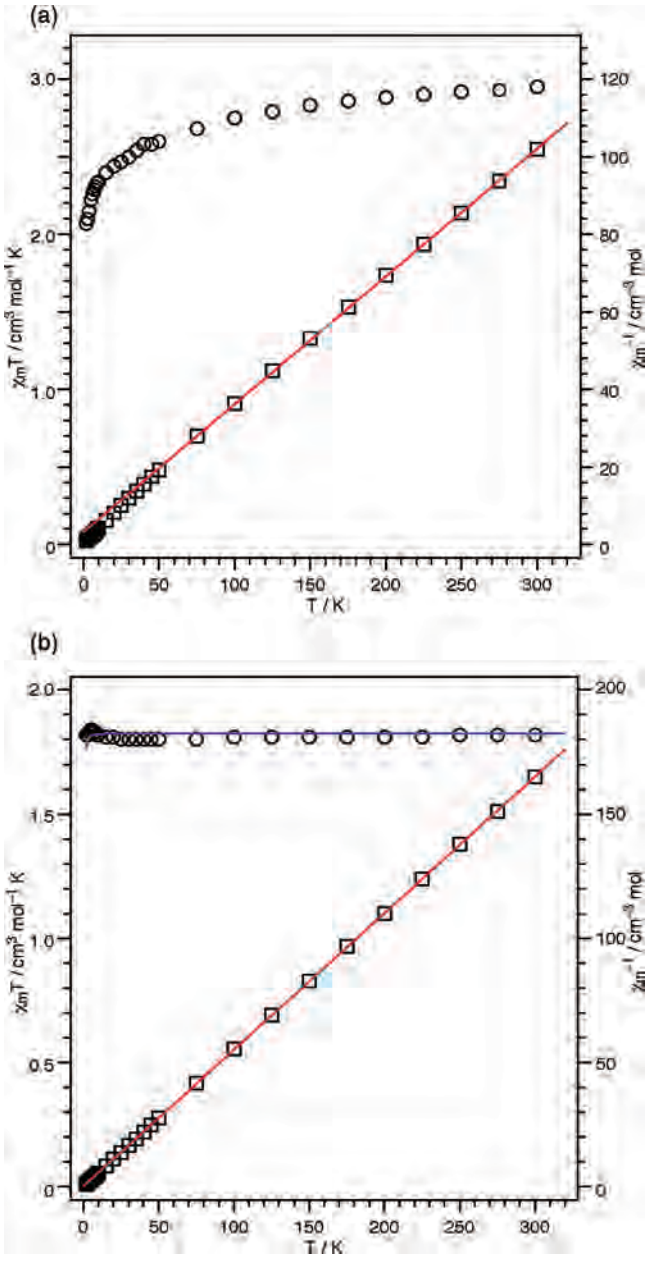

Figure 9. Plots of $\chi_m T$ (○) and χ_m^{-1} (□) for polycrystalline samples of (a) **2** and (b) **3** as a function of temperature T in an applied field of 1 kOe. The χ_m^{-1} versus T plots were analyzed by Curie−Weiss law (eq 1) with (a) $C = 3.03$ cm^3 mol^{-1} K and $\theta = -10.1$ K and (b) $C = 1.82$ cm^3 mol^{-1} K and $\theta = -0.55$ K, as shown by the red lines. The $\chi_m T$ versus T plot in (b) was fitted by using the model given in eq 2 with $D = 0.7$ cm^{-1} and $g = 1.97$, as represented by the blue line.

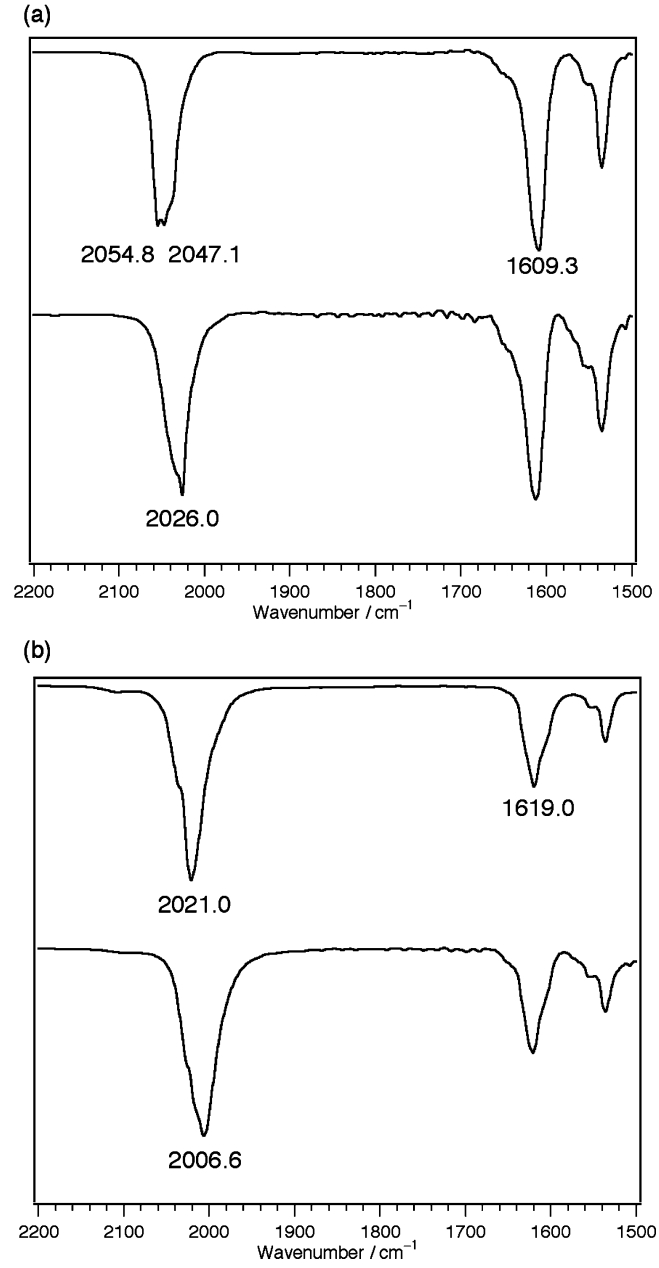

Figure 10. (a) IR spectra (KBr pellet) of $Mn^{III}(salen)(N_3)$ (**2**) (top) and $Mn^{III}(salen)(^{15}NNN)$ (bottom). (b) IR spectra (KBr pellet) of $Mn^{IV}(salen)(N_3)_2$ (**3**) (top) and $Mn^{IV}(salen)(^{15}NNN)_2$ (bottom).

Mn^{III} may mediate antiferromagnetic interactions.[26] The $\chi_m T$ versus T plot for **2** in Figure 9a shows that the $\chi_m T$ values keep decreasing in the 2−300 K range, possibly due to both zero-field splitting of the $S = 2$ ground state and an antiferromagnetic interaction between Mn^{III} centers.

As shown in Figure 10a, **2** shows IR bands at 2054.8 and 2047.1 cm^{-1}, which are shifted to 2026.0 cm^{-1} upon substitution with ^{15}NNN. A calculation by use of the simple linear triatom M1−M2−M3 model (eq 3),[27] in which the force constant (F) is assumed to have the same value for M1−M2 and M2−M3 bonds, shows that asymmetric stretching vibrations (ν_{as}) of NNN at 2054.8 and 2047.1 cm^{-1} are expected to shift to 2032.3 and 2024.7 cm^{-1} upon substitution with ^{15}NNN. Thus, the IR bands of **2** at 2054.8 and 2047.1 cm^{-1} are reliably assigned as an asymmetric azide stretch. On the other hand, the asymmetric azide stretch of **3** at 2021.0 cm^{-1} is shifted to 2006.6 cm^{-1} upon substitution with ^{15}NNN, as shown in Figure 10b. The shift of 14.4 cm^{-1} is slightly less than the value of 22.0 cm^{-1} calculated using eq 3, which is due to different F values for $N_\alpha-N_\beta$ and $N_\beta-N_\gamma$ bonds in **3**, as indicated by different bond lengths. Notably, the asymmetric azide stretches of **2** and **3** are split into at least two bands, which are separated by ∼8 cm^{-1}. Variable-temperature IR measurements from 273 to 123 K show that relative intensities of these bands do not change, although these bands are sharpened upon cooling (Figure S6 and S7, Supporting Information). This indicates that these IR bands

arise from species in a similar energy level. Splitting in the asymmetric azide stretches might be possibly due to the presence of four complexes in each asymmetric cell, which exhibit different N−N−N angles and different $N_\alpha-N_\beta$ and $N_\beta-N_\gamma$ bond lengths. Appearances of the asymmetric azide stretching bands in **2** and **3** are altered upon substitution with ^{15}NNN, due to the presence of ^{14}N- and ^{15}N-bound isomers, which may result in different splitting patterns. The IR spectrum of the CH_3CN solution of **3** shows an asymmetric azide stretch at 2023 cm^{-1} (Figure S8, Supporting Information), which is almost identical with the wavenumber of 2021 cm^{-1} in the solid state, thus suggesting that **3** is a bis-azide form also in the CH_3CN solution, just as revealed by X-ray crystallography. In contrast, **2** in CH_3CN exhibits a broadened asymmetric azide stretch at 2043 cm^{-1} (Figure S8, Supporting Information), which is shifted to a lower frequency by $\sim$7 cm^{-1} from the corresponding IR band in the solid state (2054.8 and 2047.1 cm^{-1}). The other IR bands expected for the $Mn-N_3$ unit, including the symmetric N_3 stretching, N_3 bending, and $Mn-N_3$ stretching modes,[28] could not be reliably assigned due to band overlaps. The IR band at 1609.3 cm^{-1} for **2**, which could be assigned as the C=N stretching mode, is shifted to 1619.0 cm^{-1} for **3**, although the difference of the C=N bond length is not remarkable for **2** (1.274−1.291 Å) and **3** (1.269−1.300 Å).

$$\nu_{as} = \frac{F\{b + \sqrt{(b^2 - c)}\}}{2} \quad (3)$$

$$b = \frac{1}{M1} + \frac{2}{M2} + \frac{1}{M3}$$

$$c = 4 \times \left(\frac{1}{M1 \times M2} + \frac{1}{M2 \times M3} + \frac{1}{M1 \times M3}\right)$$

Discussion

Electronic Structures of Fully-Characterized Mn^{III}(salen)$(N_3)(CH_3OH)$ versus Mn^{IV}(salen)$(N_3)_2$. As **3** is the first example of the fully characterized mononuclear Mn^{IV}(salen) complex, the electronic structures of **2** and **3** are worth comparing in detail. In the case of **2**, the $N_3-Mn^{III}-CH_3OH$ unit represents the Jahn−Teller axis of an elongated octahedron with a $Mn-N_{azide}$ bond (2.177−2.256 Å), which is comparable to the axially elongated $Mn^{III}-N_{azide}$ length (2.170 Å) but is considerably longer than the equatorial $Mn^{III}-N_{azide}$ length (1.911 and 1.951 Å) in Mn^{III}(1,4,7-triazacyclononane)$(N_3)_3$.[29] This is indicative of a singly occupied d_{z^2} orbital in the high-spin d^4 **2** (Figure 11), which is in clear contrast to the unoccupied d_{z^2} orbital in the d^3 Cr^{III}(salen)(N_3)(THF) complex bearing exactly the same salen ligand, which exhibits a shorter Cr−N bond (1.989 and 1.988 Å).[30] Complexes **2a** and **2d** with a longer $Mn-N_{azide}$ bond (2.256 and 2.221 Å) bear an almost linear N_3 ligand (178.4 and 179.8°), while the N_3 ligand in **2b** and **2c** with a shorter $Mn-N_{azide}$ bond (2.177 and 2.203 Å) is slightly bent (176.5 and 174.6°). A similar correlation between the $Mn/Cr-N_{azide}$ bond length and N−N−N angle is also found for Mn^{III}(1,4,7-triazacyclononane)$(N_3)_3$[29] and Cr^{III}(salen)(N_3)(THF).[30] The bent N_3 ligand as a consequence of a shorter $Mn/Cr-N_{azide}$ bond length is probably due to the π-back-donation from the occupied d_π orbital of Mn or Cr to the π^* orbital of the $N_\alpha-N_\beta$ double bond.

Complex **3** shows considerably shorter $Mn-N_{azide}$ bonds (1.958−2.006 Å) than **2**, suggesting removal of one electron from the d_{z^2} orbital on going from d^4 Mn^{III} to d^3 Mn^{IV} (Figure 11). The $Mn-N_{azide}$ bond length in **3** is comparable to those reported for the other Mn^{IV}-complex-bearing N_3 ligands,[18] as well as the equatorial $Mn^{III}-N_{azide}$ bond length in Mn^{III}(1,4,7-triazacyclononane)$(N_3)_3$.[29] The isoelectronic Cr^{III}(salen)$(N_3)_2$ also exhibits $Cr-N_{azide}$ bonds of a similar length (2.014 and 2.044 Å).[31] The $Mn^{IV}-N_{azide}$ bond in **3** is slightly shorter than the $Cr^{III}-N_{azide}$ bond in Cr^{III}(salen)$(N_3)_2$, which is possibly due to the higher effective nuclear charge of Mn as compared to Cr. The N_3 ligand in **3** shows bent angles of 173.5−177.4°, which are almost the same as those observed for **2b** and **2c** (176.5 and 174.6°), suggesting the contribution from the π-back-donation also in **3**. This is consistent with the electronic configuration of $(d_\pi)^1(d_\pi)^1(d_{nb})^1$ for the high-spin d^3 Mn^{IV} species.

Implications from the Solid-State Structures. The present X-ray crystallographic study of Mn^{III}(salen) and Mn^{IV}(salen) from Jacobsen's catalyst provides various conformational modes of this catalyst, depending on the electronic structure of the Mn(salen) complex. Among the X-ray crystal structures described herein, the conformation of **3** deserves particular attention from mechanistic aspects for highly enantioselective reactions by Jacobsen's catalyst, due to significantly distorted salicylidene rings by the chirality of the diimine bridge. The conformation of **3** is exactly the same as the stepped conformation, which has been previously proposed as one of the conformations of putative Mn^{V}(salen)(O) for effecting highly enantioselective oxygen transfer reactions.[12] Although **3** is not the active oxygen transfer species, the insight into the electronic nature

(22) (a) Singer, L. S. *J. Chem. Phys.* **1955**, *23*, 379–388. (b) Hempel, J. C.; Morgan, L. O.; Lewis, B. *Inorg. Chem.* **1970**, *9*, 2064–2072. (c) Pedersen, E.; Toftlund, H. *Inorg. Chem.* **1974**, *13*, 1603–1612. (d) Brown, K. L.; Golding, R. M.; Healy, P. C.; Jessop, K. J.; Tennant, W. C. *Aust. J. Chem.* **1974**, *27*, 2075–2081. (e) Richens, D. T.; Sawyer, D. T. *J. Am. Chem. Soc.* **1979**, *101*, 3681–3683. (f) Hartman, J. R.; Foxman, B. M.; Cooper, S. R. *Inorg. Chem.* **1984**, *23*, 1381–1387. (g) Pal, S.; Ghosh, P.; Chakravorty, A. *Inorg. Chem.* **1985**, *24*, 3704–3706. (h) Kessissoglou, D. P.; Li, X.; Butler, W. M.; Pecoraro, V. L. *Inorg. Chem.* **1987**, *26*, 2487–2492. (i) Chan, M. K.; Armstrong, W. H. *Inorg. Chem.* **1989**, *28*, 3777–3779.

(23) Campbell, K. A.; Yikilmaz, E.; Grant, C. V.; Gregor, W.; Miller, A.-F.; Britt, R. D. *J. Am. Chem. Soc.* **1999**, *121*, 4714–4715.

(24) Kahn, O. *Molecular Magnetism*; VCH Publisher: New York, 1993.

(25) Yuan, M.; Zhao, F.; Zhang, W.; Wang, Z.-M.; Gao, S. *Inorg. Chem.* **2007**, *46*, 11235–11242.

(26) A polycrystalline sample of **2**, which was used for a SQUID measurement, does not have a CH_3OH ligand on the sixth coordination site, as indicated by the elemental analysis of **2** after it was dried under reduced pressure.

(27) Colthup, N. B.; Daly, L. H.; Wilberley, S. E. *Introduction to Infrared and Raman Spectroscopy*, 3rd ed.; Academic Press: New York, 1990.

(28) (a) Yu, N.-T.; Tsubaki, M. *Biochemistry* **1980**, *19*, 4647–4653. (b) Czernuszewicz, R. S.; Wagner, W.-D.; Ray, G. B.; Nakamoto, K. *J. Mol. Struct.* **1991**, *242*, 99–117.

(29) Wieghardt, K.; Bossek, U.; Nuber, B.; Weiss, J. *Inorg. Chim. Acta* **1987**, *126*, 39–43.

(30) Hansen, K. B.; Leighton, J. L.; Jacobsen, E. N. *J. Am. Chem. Soc.* **1996**, *118*, 10924–10925.

(31) Darensbourg, D. J.; Mackiewicz, R. M. *J. Am. Chem. Soc.* **2005**, *127*, 14026–14038.

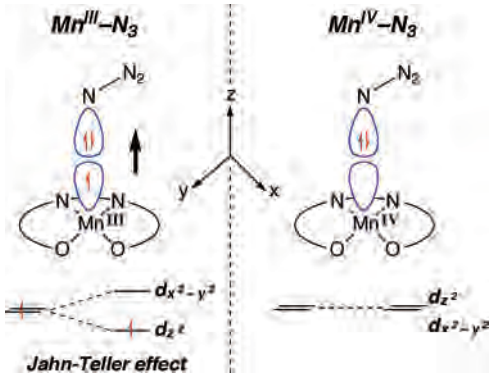

Figure 11. Electronic structures for **2** (left) and **3** (right).

and the resulting conformation of **3** would be beneficial to elucidate the conformation of putative active species such as $Mn^V(salen)(O)$.

An inspection of structural parameters for both stepped and bowl-shaped conformations shows that two axial external ligands are closely related to the conformation of the Mn(salen) molecule. Complex **3**, which bears strongly bound N_3 axial ligands, might be ideal for the stepped conformation. In contrast, **2** bears weakly coordinated N_3 and CH_3OH ligands as indicated by longer Mn−N and Mn−O bonds, which may result in crystallization as stepped and bowl-shaped conformations. The electronic structure of the Mn(salen) complex also plays a role, by affecting the coordination of external axial ligands. In the case of the d^4 Mn^{III} state, the Jahn−Teller effect is operative against a strong binding of axial ligands, thus resulting in a longer Mn−N/O distance. The d^3 Mn^{IV} species, on the other hand, are free from the Jahn−Teller effect, which enables a stronger binding of axial ligands. In accord with this idea, X-ray crystal structures of $Cr^{III}(salen)(N_3)_2$[31] and $Mn^{III}(salen)(N_3)_2$ (an azide-bridged Mn^{III} polymer)[25] show that the d^3 $Cr^{III}(salen)(N_3)_2$ complex adopts a stepped conformation just like **3**, while the d^4 $Mn^{III}(salen)(N_3)_2$ complex exhibits a rather planar conformation. A difference of the ionic radii of high-spin octahedral Mn^{III} (0.79 Å) versus Cr^{III} (0.76 Å)[32] may also contribute to the conformational difference.

By use of a computational method, Wiest and co-workers have reported an important observation that binding of a strong axial ligand to $Mn^V(salen)(O)$ induces significant deviations from a planar conformation,[13d] which might explain a positive effect of additives on both reaction rates and enantioselectivities generally observed for the Jacobsen−Katsuki epoxidation.[33] They ascribed this as a spin-state difference by binding of a strong axial ligand, which stabilizes the triplet and quintet states compared to the singlet state as the electronic structure of $Mn^V(salen)(O)$. However, we prefer to see their observation as a geometric effect rather than a spin-state difference. From our viewpoint, the main role of additives in determining the conformation of $Mn^V(salen)(O)$ is to make a balance along the axial axis by coordinating to the Mn center from the opposite side to the oxo ligand to enforce the Mn center within the N_2O_2 ligand plane, which provides an ideal coordination environment for the stepped conformation, just as described for **3**. Furthermore, the conformational difference induced by the spin state of Mn in $Mn^V(salen)(O)$ might be explained by lower $Mn-O_{oxo}$ bond orders for the triplet or quintet state than that in the singlet state. This may lead to a better balance between the oxo ligand and the opposite axial ligand.

Solution Properties. The observations in the solid state discussed in the previous section cannot necessarily correlate to the solution structures of **2** and **3**. Therefore, in this section, we discuss the solution properties of **2** and **3** with CD spectroscopy. According to the previous interpretation of CD of chiral salen complexes pioneered by Bosnich,[9,34] CD bands below 300 nm are tentatively assigned as the $\pi-\pi^*$ transition of the phenolates, while a CD band around 300−380 nm is assigned as the $\pi-\pi^*$ transition of the azomethine group. CD bands at longer wavelengths than 400 nm could not be assigned unambiguously due to an overlap of charge-transfer transitions and a d−d transition. These assignments are consistent with the observation in the present case; a negative CD band at 329 nm for the (*R*,*R*)-metal-free ligand shown in Figure S1 (Supporting Information), which arises from the $\pi-\pi^*$ transition of the azomethine group, seemingly remains intact upon the binding of Mn^{III} and Mn^{IV} ions, most probably because a relative orientation of the azomethine groups, which are directly connected to the chiral centers, are not altered significantly with or without a central metal ion. In contrast, positive−negative differential CD bands below 300 nm for the (*R*,*R*)-metal-free ligand, which arise from the $\pi-\pi^*$ transition of the phenolates, are significantly changed upon binding of a metal ion. This is possibly because the binding of a metal ion restricts a rotation around the C1−C7 and C1′−C7′ bonds, which alters a relative orientation of the phenolates.

If we could adopt this interpretation, an intense CD band at 275 nm for **3** is indicative of more chirally distorted phenolates, while a weak CD band for **2** may suggest a relatively flat arrangement of the phenolates. It is interesting to note that the intense CD band of (*R*,*R*)-**3** at 275 nm is almost comparable to those of Fox's Ni(salen)s bearing chiral substituents at the 3 and 3′ positions, which are determined to adopt a (*M*)-helix in solution.[17] A similarity of CD at 275 nm suggests the phenolates in (*R*,*R*)-**3** might be twisted in a (*M*)-helical manner, possibly in addition to the stepped conformation in solution (Figure 12). An inversed sign of 275 nm CD for (*S*,*S*)-**3** suggests a twist of the phenolates for (*P*)-helix in solution. In contrast, CD bands of **3** at 300−380 nm are weaker in magnitude than those of Fox's Ni(salen)s, possibly because Fox's Ni(salen)s have additional large chiral substituents at the 3 and 3′ positions, which might affect the arrangement of the azomethine groups. Fox and

(32) Shannon, R. D. *Acta Crystallogr.* **1976**, *A32*, 751–767.
(33) (a) Irie, R.; Ito, Y.; Katsuki, T. *Synlett* **1991**, 265–266. (b) Finney, N. S.; Pospisil, P. J.; Chang, S.; Palucki, M.; Konsler, R. G.; Hansen, K. B.; Jacobsen, E. N. *Angew. Chem., Int. Ed.* **1997**, *36*, 1720–1723.
(34) (a) Bosnich, B. *J. Am. Chem. Soc.* **1968**, *90*, 627–632. (b) Downing, R. S.; Urbach, F. L. *J. Am. Chem. Soc.* **1969**, *91*, 5977–5983. (c) Boucher, L. J.; Herrington, D. R. *Inorg. Chem.* **1974**, *13*, 1105–1108. (d) Pasini, A.; Gullotti, M.; Ugo, R. *J. Chem. Soc., Dalton Trans.* **1977**, 346–356. (e) Carroll, K. M.; Schwartz, J.; Ho, D. M. *Inorg. Chem.* **1994**, *33*, 2707–2708. (f) Chang, C. J.; Connick, W. B.; Low, D. W.; Day, M. W.; Gray, H. B. *Inorg. Chem.* **1998**, *37*, 3107–3110.

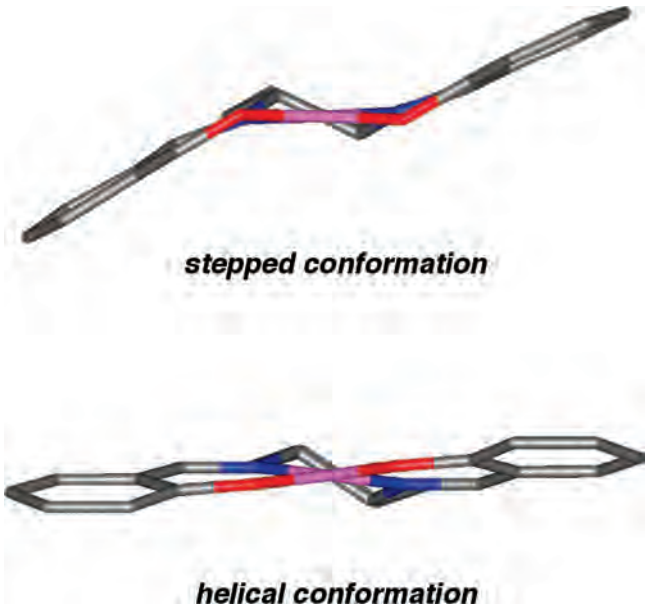

Figure 12. Stepped and helical conformation models, which were created using coordinates of **3** and Fox's Ni(salen),[17] respectively.

co-workers found that a *trans*-cyclohexanediamine moiety in salen complexes alone is not enough to induce a chiral twist in phenolates without a chiral auxiliary at the 3 and 3′ positions.[17] Their finding indeed applies to **2**, but not to **3**, bearing helically twisted phenolates by *trans*-cyclohexanediamine as an only chiral unit. We hypothesize that axial external ligands in **3** might play a role in transmitting chirality from a *trans*-cyclohexanediamine moiety to phenolates in solution, but the hypothesis needs further experimentation. Separated ^{1}H NMR signals for 4/4′H and/or 6/6′H for **2** and **3** indicate an absence of *C*2 symmetry about two phenolates.

Temperature-dependent CD spectra with isodichroic points in the range from 298 to 253 K (Figure 5b) indicate that the solution of **3** contains two conformers equilibrating at room temperature. At lower temperatures below 253 K, no further temperature dependence is observed for the CD spectrum of **3**, suggesting that one of two conformers showing this CD spectrum is predominant below 253 K. On the other hand, a CD spectrum at temperatures high enough to induce no further change should arise from a nearly 1:1 mixture of two conformers, but unfortunately we cannot measure variable-temperature CD spectra at temperatures above 313 K due to the decomposition of **3**. Although a detailed description for the equilibrium by thermodynamic parameters is not possible without information on the conformer in a higher energy level, a rather small change for CD spectra in the range from 298 to 253 K might suggest that the equilibrium predominantly favors the formation of a low-energy conformer with more chiral distortion even at room temperature. Equilibrium between two conformers as revealed by variable-temperature CD is not apparent from a variable-temperature ^{1}H NMR experiment, and only one set of signals is observed for **3** in the range from 298 to 253 K, as shown in Figure 6b. This is partly because an exchange rate between two conformers is fast for **3**, as compared with Fox's Ni(salen)s bearing a larger substituent at the 3 and 3′ positions, which were reported to show a chemical exchange with coalescence at 253 K.[17] A paramagnetic nature of **3** also affects an observation of a chemical exchange by NMR spectroscopy.

Conclusion

The present X-ray crystallographic study provides the first example of a chirally distorted stepped conformation of a Mn complex of Jacobsen's salen ligand. External axial ligands play a pivotal role for the formation of the rigid stepped conformation. When the Mn(salen) complex bears weakly bound axial ligands, the Mn center remains mobile around the basal N_2O_2 ligand plane, resulting in a relatively flat conformation. In contrast, external axial ligands, which coordinate to the Mn center in an equally strong manner from both sides, enforce the Mn center within the basal N_2O_2 ligand plane, leading to the rigid conformation distorted by the chirality of the diimine bridge. A higher-valent Mn center including Mn^{IV} and Mn^{V} is advantageous in this regard due to absence of the Jahn−Teller effect. It is suggested that, also in solution, **3** may adopt a more chirally distorted conformation compared to **2**. The insight into the conformation of Mn(salen) described herein would apply equally to the long-sought but still unknown active species in Jacobsen−Katsuki enantioselective epoxidation.

Experimental Section

Caution! *The azide complexes* **2** *and* **3** *are potentially explosive and should be handled only in small amounts with appropriate care.* We have not encountered any problem in handling **2** and **3** on a 100 mg scale, including evaporation of the solvent, preparation of ground samples, and heating at 80 °C in vacuo for removing the incorporated solvent.

Instrumentation. Cyclic voltammograms were measured with an ALS612A electrochemical analyzer (ALS). A saturated calomel reference electrode, a glassy carbon working electrode, and a platinum-wire counter electrode were utilized. Measurements were carried out for the 1×10^{-3} M solution in anhydrous CH_3CN containing 0.1 M Bu_4NClO_4 at a scan rate of 50 mV s^{-1} at room temperature under an Ar atmosphere. The *E* values were referenced to the $E_{1/2}$ value of ferrocene, which was measured under identical conditions. UV−vis spectra were recorded for the 4×10^{-5} M solution in spectrophotometric-grade CH_3CN in a quartz cell (l = 1 cm) on an Agilent 8453 spectrometer (Agilent Technologies). Controlled-potential electrochemical reduction was conducted for the 5×10^{-4} M CH_3CN solution containing 0.1 M Bu_4NClO_4 under an Ar atmosphere at room temperature in a thin-layer quartz cell (l = 0.05 cm) using a gold-mesh working electrode, a platinum-wire counter electrode, and a Ag/AgCl reference electrode, which are connected to a HA-151 potentiostat-galvanostat (HOKUTO DENKO). EPR spectra were recorded for 30 μL of the 0.01 M solution in a quartz cell (d = 5 mm) on an E500 continuous-wave X-band spectrometer (Bruker) with an ESR910 helium-flow cryostat (Oxford Instruments). Measurements were made under the following conditions: microwave frequency, 9.56 GHz; microwave power, 2.012 mW; modulation amplitude, 7 G; time constant, 163.84 ms; conversion time, 163.84 ms. ESI-MS spectra were obtained for the CH_2Cl_2 solution at a cone voltage of 10 V with an LCT time-of-flight mass spectrometer equipped with an electrospray ionization interface (Micromass). IR spectra were measured for the KBr pellet in a homemade sample folder on an FT/IR-460Plus (JASCO)

equipped with a USP-203 low-temperature chamber (UNISOKU). IR spectra were measured for the CH_3CN solution using a FLAB50-UV-01 demountable flow-through cell (GL Sciences Inc.). IR optical windows made of KRS-5 (Pier Optics Co., Ltd.) were utilized for the low-temperature chamber and the flow-through cell. Measurements were done under the following conditions: accumulation, 32 times; resolution, 4 cm^{-1}. CD spectra at room temperature were recorded in a quartz cell ($l = 1$ cm) on a J-720W spectropolarimeter (JASCO). In the case of variable-temperature measurements, a quartz cell ($l = 0.05$ cm) and a USP-203 low-temperature chamber (UNISOKU) were employed. Measurements were done under the following conditions: scan rate, 100 nm min^{-1}; bandwidth, 5.0 nm; response, 4 s; resolution, 1 nm. Elemental analyses were conducted on a CHN corder MT-6 (Yanaco). The 500 MHz NMR spectra were measured on an LA-500 spectrometer (JEOL).

Magnetic Susceptibility. Solid-state magnetic susceptibility measurements were made by using a MPMS-7 SQUID susceptometer (Quantum Design) operating in the temperature range 2−300 K. Well-ground polycrystalline samples were wrapped in a plastic sheet and were loaded into the sample folder (a drinking straw). The susceptibility of the plastic sheet and the sample folder was measured in the same temperature range and field, to provide an accurate correction for its contribution to the total magnetic susceptibility. Diamagnetic corrections of -4.10×10^{-6} and -4.23×10^{-6} cm^3 mol^{-1} were estimated from Pascal constants for **2** and **3**, respectively.[24]

X-Ray Crystallography. Measurements were made on a Rigaku/MSC Mercury CCD diffractometer equipped with graphite monochromated Mo Kα radiation ($\lambda = 0.71070$ Å). Data were collected at 173 K under a cold nitrogen stream. All crystals were mounted on a glass fiber using epoxy glue. The images were processed with the CrystalClear program (version 1.3.5).[35] The structures were solved by the direct method using SHELXS-97[36,37] and refined by full-matrix least-squares procedures on F^2 using SHELXH-97,[36,38] on the CrystalStructure software package (version 3.8.2).[39] Anisotropic refinement was applied to all non-hydrogen atoms. Hydrogen atoms were placed at the calculated positions and refined with isotropic parameters. Corrections for Lorentz-polarization effects and absorption were performed. The Flack parameters[40] were calculated for **2** and **3** to confirm the absolute configuration. We were only able to refine **2** and **3** to *R* values of 6.67 and 8.28%, respectively. Rather high *R* values are due to a failure to resolve the *tert*-butyl groups and the solvent molecules incorporated in the crystal. The poorly resolved *tert*-butyl groups cause the Checkcif program provided by the International Union of Crystallography to point A-level alerts associated with this problem. Nevertheless, the geometries about the salen complexes are well-defined. The structural parameters including α, β, and γ and the $Mn-N_2O_2$-plane distance were obtained using the crystal structure visualization and exploration program Mercury (version 1.4.2), provided by the Cambridge Crystallographic Data Center.

Materials. CH_2Cl_2, CH_3OH, CH_3CN, and toluene were purchased from Kanto as anhydrous solvents and were utilized as received. For UV−vis and CD measurements, spectrophotometric-grade CH_3CN was utilized as received from Wako. Bu_4NClO_4 was purchased from Kanto and was dried in vacuo in the presence of P_2O_5. *m*-CPBA was purchased from Nacalai and was purified by washing with a phosphate buffer.[41] The purity of *m*-CPBA was checked with iodometry. (*R*,*R*)- and (*S*,*S*)-*N*,*N*′-bis(3,5-di-*tert*-butylsalicylidene)-1,2-cyclohexanediaminomanganese(III) chlorides, (*R*,*R*)-*N*,*N*′-bis(3,5-di-*tert*-butylsalicylidene)-1,2-cyclohexanediamine), 18-Crown-6 (≥99.5%) and NaOTf (98%) were purchased from Aldrich and were used as received. NaN_3 was purchased from Wako, and $Na^{15}NNN$ (99 atom %) was purchased from ICON.

Synthesis of 2. NaN_3 (132 mg, 2 mmol) in distilled water (2 mL) was added to a solution of **1** (635.2 mg, 1 mmol) in CH_2Cl_2 (10 mL) and CH_3OH (10 mL). The resulting solution was stirred for 1 h at room temperature. Then, the solvent was removed by rotary evaporation, and the residue was dried in vacuo. The crude product was dissolved in anhydrous CH_2Cl_2, and the solution was filtered through a pad of celite and was then passed through a membrane filter (Cosmonice Filter S, Nacalai). The CH_2Cl_2 solvent was removed by rotary evaporation, and the product was dried in vacuo. Crystallization from hot CH_3CN yielded **2** (578 mg, 0.90 mmol). The crystal suitable for the X-ray crystallographic analysis was obtained by crystallizing (*R*,*R*)-**2** (10.0 mg, 16 μmol) from the hot CH_3OH-H_2O solution (8:1, 10 mL) in the presence of NaN_3 (10.4 mg, 160 μmol) and 18-crown-6 (42.3 mg, 160 μmol). Anal. calcd for $C_{36}H_{52}N_5O_2Mn$: C, 67.37; H, 8.17; N, 10.91. Found: C, 67.18; H, 8.26; N, 10.80.

Synthesis of 3. To a solution of **2** (641.8 mg, 1 mmol) in CH_3CN (50 mL) and distilled water (5 mL) was added *m*-CPBA (172.6 mg, 1 mmol) as a solid and NaN_3 (650.1 mg, 10 mmol) in distilled water (2 mL) at 263 K. The resulting solution was stirred at 263 K for 1 h, and then the solvent was removed at the same temperature in vacuo. The residue was dissolved in CH_2Cl_2 under ambient conditions, and the solution was filtered through a pad of celite and was then passed through a membrane filter (Cosmonice Filter S, Nacalai). Crystallization from CH_2Cl_2 (∼10 mL) and pentane (50 mL) at 253 K gave **3** (537 mg, 0.79 mmol). The crystal suitable for X-ray crystallographic analysis was obtained by crystallizing (*R*,*R*)-**3** (10.0 mg) from CH_2Cl_2 (2 mL) and pentane (10 mL) at 253 K. Anal. calcd for $C_{36}H_{52}N_8O_2Mn$: C, 63.23; H, 7.67; N, 16.39. Found: C, 63.14; H, 7.64; N, 16.38.

Acknowledgment. We thank Mr. Seiji Makita (IMS) for elemental analysis. This work was supported by grants from the Japan Science and Technology Agency, CREST.

Supporting Information Available: An X-ray crystallographic file in CIF format for (*R*,*R*)-**2** and (*R*,*R*)-**3**. Figures S1−S8. This material is available free of charge via the Internet at http://pubs.acs.org.

IC800443Q

(35) (a) *CrystalClear 1.3.5 SP2*; Rigaku and Molecular Structure Corp.: The Woodlands, TX, 2004. (b) Pflugrath, J. W. *Acta Crystallogr.* **1999**, *D55*, 1718–1725.
(36) Sheldrick, G. M. *Acta Crystallogr.* **2008**, *A64*, 112–122.
(37) Sheldrick, G. M. *SHELXS-97, Program for Crystal Structure Solution*; University of Göttingen: Göttingen, Germany, 1997.
(38) Sheldrick, G. M. *SHELXH-97, Program for Refinement of Crystal Structures*; University of Göttingen: Göttingen, Germany, 1997.
(39) (a) *CrystalStructure 3.8.2: Crystal Structure Analysis Package*, version 3.8.2; Rigaku and Rigaku/MSC: The Woodlands, TX, 2007. (b) Watkin, D. J.; Prout, C. K.; Carruthers, J. R.; Betteridge, P. W. *Crystals, Issue 10*; Chemical Crystallography Laboratory: Oxford, U.K., 1996.
(40) Flack, H. D. *Acta Crystallogr.* **1983**, *A39*, 876–881.
(41) Schwartz, N. N.; Blumbergs, J. H. *J. Org. Chem.* **1964**, *29*, 1976–1979.